Biomaterials 35 (2014) 1402–1410

Contents lists available at ScienceDirect

Biomaterials

journal homepage: www.elsevier.com/locate/biomaterials

Genetically encoded FRET-based biosensor for imaging MMP-9 activity

Michal Stawarski [a], Izabela Rutkowska-Wlodarczyk [a], André Zeug [b], Monika Bijata [a], Hubert Madej [c,a], Leszek Kaczmarek [a], Jakub Wlodarczyk [a,*]

[a] Department of Molecular and Cellular Neurobiology, The Nencki Institute of Experimental Biology, ul. Ludwika Pasteura 3, Warszawa 02-093, Poland
[b] Department of Cellular Neurophysiology, Hannover Medical School, Carl-Neuberg-Strasse 1, Hannover 30625, Germany
[c] Department of Biophysics, Warsaw University of Life Sciences, ul. Nowoursynowska 166, Warszawa 02-787, Poland

ARTICLE INFO

Article history:
Received 18 October 2013
Accepted 11 November 2013
Available online 26 November 2013

Keywords:
Förster resonance energy transfer (FRET)
Matrix metalloproteinase 9
Biosensors
Quantitative microscopy
Long-term memory
Cancer-related processes

ABSTRACT

A genetically encoded Förster Resonance Energy Transfer (FRET)-based biosensor that continuously monitors matrix metalloproteinase 9 (MMP-9) activity was developed. MMP-9 is an extracellularly acting endopeptidase with a prominent role in development, learning and memory, cancer metastasis, and stroke. To assess the biological function of the protease, determining the precise kinetics and localization of MMP-9 activity is required. The nontoxic, genetically encoded FRET biosensor presented herein is anchored in the cellular membrane and thus provides an important advantage over currently employed probes. The biosensor allows the study of the proteolytic activity of MMP-9 with high temporal and subcellular resolution at the precise region of MMP-9 action on the cell. The applicability of the biosensor both *in vitro* and in living cells was demonstrated by ratiometrically analyzing the cleavage of the biosensor by a purified auto-activating mutant of MMP-9 and endogenously secreted protease in cultured tumor and neuronal cells. The precise kinetics of endogenous MMP-9 activity was measured, which demonstrates in a straight-forward manner the applicability of the biosensor concept.

1. Introduction

Advances in elucidating the mechanisms that govern basic cellular functions have allowed a shift of researchers' attention to cellular dynamics, creating a growing demand for methods that are sensitive and sufficiently quick to track dynamic processes within living cells. In the area of the subcellular spatiotemporal localization of macromolecule interactions, Förster Resonance Energy Transfer (FRET)-based approaches are particularly useful. Recent years have witnessed a growth in the number and diversity of genetically encoded FRET-based biosensors that have been developed. They can be used to study such diverse phenomena as ion concentration [1–3], organic compound concentration [4], guanosine triphosphatase activity [5], protein phosphorylation [6] and mechanical stress within a cell [7], and enable tracking these phenomena in real time in living cells and organisms.

Matrix metalloproteinase 9 (MMP-9) is an extracellularly secreted 92 kDa protease that belongs to a family of zinc- and calcium-dependent endopeptidases. It cleaves several extracellular matrix proteins and cell adhesion molecules. Research indicates that MMP-9 plays a significant role in the development of cancer through its dual role of regulating angiogenesis and cleaving the extracellular matrix, thus enabling tumors to enter metastasis [8–10]. An increase in MMP-9 expression was observed in a number of different tumors compared with healthy subjects, with an apparent positive association between tumor aggressiveness and MMP-9 activity levels [11,12]. The MMP-9-regulated processing of the extracellular matrix may also lead to the release of cytokines and growth factors [13,14] that facilitate angiogenesis. MMP-9 activity levels may be a prognostic factor in cancer (see review [15]).

MMP-9 appears to be one of the key regulators in synaptic plasticity that underlies learning and memory [16–19] and the formation and maintenance of dendritic spines that harbor excitatory synapses [20–22]. Several recent reports have demonstrated the importance of MMP-9 and its pivotal functional role in physiological long-term potentiation (LTP; an experimental paradigm that mimics plasticity) in diverse brain regions [23]. Both MMP-9 protein levels and proteolytic activity were rapidly increased by stimuli that enhance neuronal activity [17,24–26].

* Corresponding author. The Laboratory of Cell Biophysics, Department of Molecular and Cellular Neurobiology, The Nencki Institute of Experimental Biology, ul. Ludwika Pasteura 3, Warszawa 02-093, Poland. Tel.: +48 225892360; fax: +48 228225342.
E-mail address: j.wlodarczyk@nencki.gov.pl (J. Wlodarczyk).

0142-9612/$ – see front matter © 2013 Elsevier Ltd. All rights reserved.
http://dx.doi.org/10.1016/j.biomaterials.2013.11.033

Commonly employed methods of detecting the proteolytic activity of MMP-9 such as gel and *in situ* zymography (based on dye-quenched [DQ]-gelatin, a fluorogenic substrate for gelatinases), do not allow the high-resolution localization of gelatinase activity. Because they are freely diffusive probes, the localization of fluorescence readout is limited in terms of spatial and temporal resolution. Moreover, they are both gelatin-based assays, and they detect the activity of other gelatinases, particularly MMP-2. The expression levels of MMP-2 are much higher than those of MMP-9, and the majority of cleavage detected by these methods reflects the proteolytic activity of MMP-2 rather than MMP-9.

Several fluorescence-based MMP-9 activity biosensors have been developed in recent years [27–32]. Because of the potential of MMPs as prognostic markers of cancer, considerable work has been performed in the area of diagnostic and analytical probes for the detection of the proteolytic activity of MMP-9 in cancer (see Ref. [29] for a survey of several MMP-9 activity probes and their suitability for cancer detection; see Ref. [33] for a review of the detection of MMP activity in cancer; see Refs. [28,34–36] for near-infrared probes developed for *in vivo* imaging). The genetically encoded FRET-based MMP-9 activity biosensor described herein overcomes the limitations of the currently available biosensors and allows the study of the fundamental physiological and pathological roles of MMP-9 in living cells.

2. Materials and methods

The biosensor contains one donor fluorescent protein and two acceptor fluorescent proteins to increase the FRET efficiency of the biosensor. The linker between the donor and acceptor proteins contains specific MMP-9 cleavage sequence [37] (the specificity has been tested elsewhere [27,38]). The entire biosensor is anchored in the plasma membrane by a transmembrane domain of the platelet-derived growth factor receptor to prevent diffusion and allow the readout of activity with high spatial resolution.

2.1. Gene construction

The genetically encoded FRET-based MMP-9 activity biosensor was assembled in pDisplay plasmid (Clontech). The mTFP1 gene was amplified from the pmTFP1-N1 plasmid (Allele Biotech). The plasmid that encodes the Venus gene (a variant of EYFP first described in Ref. [39] that carries mutations that increase the maturation rate) was a generous gift of Jacek Jaworski, (The International Institute of Cell Biology, Warsaw, Poland). The enzymes used for cloning were purchased either from New England Biolabs or Thermo Scientific.

The biosensors were cloned using SLIC cloning methodology described elsewhere [40]. Venus and mTFP1 were amplified with Phusion Hot Start II High Fidelity Polymerase. The primers used for fluorescent protein gene amplification contained long overhangs at their 5′ ends that were complementary either to the pDisplay plasmid (Venus2 and mTFP1 [forward and reverse primers, respectively]) or to the downstream nucleotide sequence of the biosensor (Venus2 and mTFP1 [reverse and forward primers respectively]; Venus1 [both primers]). The pDisplay plasmid was cleaved with XmaI and SacII enzymes to generate single-stranded ends. Two restriction enzyme sites were introduced into the tandem construct: the NheI site separated fluorescent proteins Venus1 and Venus2 and the AflII site was cloned between the Venus1 and mTFP1 genes. An oligonucleotide (linker LN1) with the following sequence was cloned into the AflII site: CTTAAGG-GATCCCCCCGCTCTCTCTCTAAGCTTAAA-(GGAGGAACCGGTGGAACT)$_8$-CTTAAG (the genetic sequence of MMP-9 cleavage site is underlined). The following oligonucleotide (linker LN2) was cloned into the NheI site: GCTAGCGGTGGTAGCGGTGG-TAGCGGTGCTAGT-(GGTGGTTCTGGTTCTAGA)$_8$-GCTAGC. LN1 and LN2 oligonucleotides were composed of identical segments separated by restriction sites (LN1 – AgeI, LN2 – XbaI) to facilitate the rapid adjustment of the length of the linkers.

The biosensor constructed in the following fashion carried the MMP-9 cleavage site within an unstructured loop. This biosensor was referred to as a biosensor with a loop-like linker.

The biosensor with the MMP-9 cleavage site located within the α-helical structure was prepared by replacing the LN1 linker with the following sequence: CTTAAGGAGGAGGAGATCAGAGAGGCCTTCAGAGTGTTCCCCAGAAGCCTGAGCCTGA-GACACGTGATGACCAACCTGCTTAAG (the genetic sequence of the MMP-9 cleavage site is underlined). This biosensor was referred to as a biosensor with a helical linker.

To generate the membrane-anchored mTFP1, the mTFP1 gene was amplified with primers that carried ApaI and BglII restriction sites on 5′ overhangs and cloned in the pDisplay plasmid linearized with the same restriction enzymes. Variant biosensors with shorter linkers were derived from a full length biosensor by the partial cleavage of the LN1/LN2 linkers with AgeI or XbaI. Thirty-eight biosensor variants were created.

2.2. Cell culture and transfection

HEK293 cells were cultured in Dulbecco's Modified Eagle Medium (DMEM 4.5 g/l glucose) supplemented with 10% FBS and 1% P/S at 37 °C in 5% CO_2. Plasmids that encoded the biosensors were purified with the Endo Free Plasmid Maxi Kit (Qiagen). The cells were transfected with polyethyleneimine (PEI; 5 μg/μl) for 4 h. The cells that were intended to be imaged on confocal microscope, were cultured on glass cover slips.

Hippocampal and cortical primary cell cultures were prepared from WISTAR rat pups as described previously [26]. Hippocampal neurons were transfected with Effectene (Qiagen) reagent according to the protocol provided by the supplier (12-well format) with the following modifications: the amount of the Effectene reagent was lowered to 5.5 μl, 200 μl of fresh growth medium was added to the transfection mix, and the cells were incubated for 45 min with the transfection medium, after which the old growth medium was returned. The cell culture reagents were acquired from Sigma–Aldrich.

2.3. Cell imaging

For Acceptor-Photobleaching (AP), the cells were fixed 2 days post-transfection with 4% paraformaldehyde and 3% sucrose in 1× PBS. The experiments were performed on a Leica SP5 microscope equipped with 63× NA (1.4) oil-immersion objective. Images were acquired at 1024 × 1024 pixel resolution. For FRET efficiency determination, the Venus was bleached with a 514 nm laser, and both proteins were imaged by exciting them with a 458 nm argon laser line. Biosensors that were determined to have the highest FRET efficiency were further analyzed using Fluorescence Lifetime Imaging Microscopy (FLIM). To perform FLIM, we used a Becker & Hickl system (Berlin, Germany). Two-photon time-domain images were acquired using a TCS SP2 confocal laser scanning microscope (Leica) with a femtosecond-pulsed Ti:Sapphire laser (Mai-Tai Spectraphysics). Time-resolved fluorescence decay was acquired by time-correlated single-photon counting (TCSPC) using an R3809U-50 detector (Hamamatsu Photonics, Herrsching am Ammersee, Germany) and SPC830 acquisition board (Becker &Hickl). The FRET efficiency was calculated as the average of 10 regions of interest (ROI) per picture, based on the double exponential fluorescence decay model fitted with the use of SPC-IMAGE software (Becker & Hickl).

For spectral analysis, lambda stacks were acquired on a Zeiss LSM780 microscope equipped with 63× NA (1.4) oil-immersion objective at 1024 × 1024 pixel resolution. The biosensor was excited with a 458 nm argon laser, and 32 lambda channels were acquired at 9 nm steps. The acquired datasets were analyzed using Fiji ImageJ software by measuring the average fluorescence intensity of the plasma membrane in each channel. Recovered biosensor fluorescence emission spectra were normalized to the unit area.

For live-cell imaging, the HEK293 cells were cultured on Glass Bottom Microwell Dishes (MatTek Corporation). Two days post-transfection the cells were imaged on a Zeiss LSM780 microscope fitted with an incubator and equipped with a water-immersion 40× objective. A single optical section of the cells was captured at 1024 × 1024 pixel resolution every 30 s, with linear unmixing of the donor and acceptor fluorescence performed in real time. Acquisition was performed for 30 min. Five minutes after the start of image acquisition, the cells were either mock-treated (with pure growth medium) or an auto-activating (aaMMP-9) or inactive (inMMP-9) form of MMP-9. Stimulation was performed using MMP-9 at a final concentration of 460 ng/ml aaMMP-9 [41] and inMMP-9 [42] were designed and purified as described previously. The data analysis was performed using custom software within the Matlab suite. The Venus-to-mTFP1 fluorescence intensity ratio was calculated for each pixel and plotted against the time elapsed from the start of the experiment.

Live-cell imaging of hippocampal neurons was performed 2 days post-transfection (9 days *in vitro*) using a Zeiss confocal microscope fitted with an incubator and equipped with Spinning Disc. Coverslips with hippocampal neurons were mounted in a custom-made chamber and imaged with a water-immersion 40× objective. The biosensor was excited with a 405 nm laser line. mTFP1 and Venus were imaged separately, with z-stacks acquired for both channels every minute. Five minutes after the beginning of the experiment, the cells were treated in one of the following ways: aaMMP-9 was added to a final concentration of 400 ng/ml, mock treatment was performed or the cells were stimulated with the cLTP mixture (i.e., 50 μM forskolin, 50 μM picrotoxin, 0.1 μM rolipram to chemically induce LTP [43]. The data analysis was performed using a custom software within the Matlab suite. The Venus-to-mTFP1 fluorescence intensity ratio was calculated for each pixel, and the time course of the ratio was plotted.

2.4. Acceptor-photobleaching/fluorescence lifetime imaging microscopy

The apparent FRET efficiency value of variant biosensors from AP data was calculated using the following equation: $Ef_D = 1 - (F_{DA}/F_D)$. f_D is the fraction of donor that participates in the FRET complex. F_{DA} and F_{DA} are the background-subtracted and acquisition bleaching-corrected pre- and post-bleach mTFP1 fluorescence

intensities, respectively. The acquisition bleaching-corrected post-bleach mTFP1 intensities were calculated as the following: $F_D = F_D^{B,post} + F_D^{B,pre}(F_D^{R,pre} - F_D^{R,post})/F_D^{R,pre}$. F_D^B and F_D^R refer to the mTFP1 intensities of the bleach and reference ROI, and *pre* and *post* refer to pre-bleach and post-bleach measurements.

FRET efficiency values from FLIM data were calculated with the following equation: $Ef_D = A_{DA}(1 - \tau_D/\tau_{DA})/(A_{DA} + A_D)$. τ_D is the lifetime of the donor in the absence of the acceptor (in our case the membrane-anchored mTFP1). τ_{DA} is the lifetime of the FRET-based MMP-9 activity biosensor. A_{DA} and A_D are the amplitudes of individual decay components [44]. Error values were estimated using the Gaussian noise propagation equation:

$$\mathrm{stdE} = \sqrt{\left[(\partial E/\partial\tau_D)^2\Delta\tau_D^2 + (\partial E/\partial\tau_{DA})^2\Delta\tau_{DA}^2\right]}$$

2.5. HEK293 cell fractioning

Cell fractioning experiments were performed using the ProteoExtract Subcellular Proteome Extraction kit (Calbiochem). The myc-tagged biosensor (myc-tag originates from the pDisplay plasmid) was detected using Western blot with anti-myc antibody (Santa Cruz Biotechnologies, #sc-40). Fraction purity was tested using Western blot with the following antibodies: anti-hsp90 (Stressgen, #SPS-771), anti-N-cadherin (BD Biosciences, #610920), and anti-histone H3 (Abcam, #ab10799).

2.6. In vitro cleavage of the biosensor

Two days post-transfection HEK293 cells were washed once with 1× PBS, scraped from the plate, and lysed for 1 h at 4 °C in 50 mM Tris-Cl (pH 7.5), 1% Triton X-100, 10 mM $CaCl_2$, 0.02% NaN_3 and 1 μM $ZnCl_2$ without protease inhibitors. The lysate was then centrifuged at 13,400 rotations per minute for 15 min at 4 °C. Equal amounts of the cleared lysate were used in the subsequent reactions. aaMMP-9 and inMMP-9 were used at 10 μg/ml concentrations. The GM6001 inhibitor was used at a 25 μM concentration. The reactions were stopped at 30 min, 1 h, 4 h or after overnight incubation at 37 °C with the addition of SDS-PAGE Sample Buffer and heated to 100 °C for 10 min. The biosensor was detected using Western blot with anti-green fluorescent protein (GFP) antibody (MBL, #598).

2.7. Cleavage of the biosensor in the cell culture

Two days after transfection of HEK293 cells, the culture medium was replaced by pure DMEM. The cells were incubated for 30 min with 800 ng/ml aaMMP-9 and then fixed with 4% PFA and 3% sucrose in 1× PBS. Lambda stack images were acquired as previously described.

2.8. Western blot

The detection of β-dystroglycan (βDG) cleavage in cortical neurons following chemically induced LTP (cLTP) with the Western blot assay was performed as described previously [26]. The cells were collected after 2, 5, 7, 10, 15, 20 or 30 min incubation with the cLTP mixture to obtain the detailed kinetics of βDG cleavage by endogenous MMP-9.

2.9. Statistical analysis

The statistical values are expressed as mean ± standard error of the mean (SEM). The statistical analyses were performed using Microsoft Excel, and the datasets were tested using Student's *t*-test. Indications of significance correspond to $p < 0.05$ (*) and $p < 0.01$ (**).

3. Results

3.11. Structure of the biosensor

The MMP-9 biosensor presented herein is a chimeric protein, consisting of a transmembrane domain, Teal fluorescent protein, a cleavage site specific for MMP-9, and two tandem Venus proteins (indicated as Venus1 and Venus2 in Fig. 1A). The signal peptide at the *N*-terminus of the biosensor directs the protein to the secretory pathway. Fluorescent proteins are separated by linkers that were optimized in length to ensure the highest FRET efficiency. The MMP-9 cleavage site is located within the linker that separates Venus1 and mTFP1. The c-myc tag is located at the *C*-terminus of the biosensor. The MMP-9 cleavage of the biosensor leads to conformational changes, separation of the acceptor proteins from the donor, and a decrease in FRET observed as a drop in the acceptor-to-donor fluorescence intensity ratio.

A screen of known MMP-9 substrates yielded neither a consensus sequence nor a secondary structure assumed by the MMP-9 cleavage site, but Kridel et al. [37] reported a family of short peptides that are cleavable by MMP-9. The consensus *N*′-PRSLS-*C*′ sequence suggested therein Ref. [37] was cloned into the biosensor. Previous work by Fudala et al. [27] showed that this sequence is indeed recognized by MMP-9. The specificity of the cleavage sequence was shown previously in Refs. [27,38] using human recombinant pro-MMP-2, pro-MMP-3, and pro-MMP-7.

To provide high differences in the acceptor-to-donor fluorescence ratio, mTFP1 [45] was chosen as a FRET donor for the MMP-9 activity biosensor. mTFP1, shown to have improved spectral properties compared with Cyan Fluorescent Protein, forms a more efficient FRET pair with the Yellow Fluorescent Protein (YFP) [45]. Venus, an improved variant of YFP, was selected as the FRET acceptor.

Although the majority of FRET-based biosensors contain one donor protein and one acceptor protein, dual acceptors principally improve the FRET efficiency of FRET biosensors. FRET efficiency of a single donor and single acceptor system is defined as: $E_1 = k_T/(k_T + k_R + k_F)$, in which k_T is the energy transfer rate, k_R is the rate constant of all other deactivation processes and k_F is the fluorescence decay rate. The FRET efficiency of a single donor and two acceptors system is given by the following equation: $E_2 = 2k_T/(2k_T + k_R + k_F)$. Introduction of a second acceptor in a FRET biosensor increases its FRET efficiency, because $E_2 = 2E_1/(1 + E_1) \geq E_1$. Therefore, dual acceptors were incorporated into the biosensor. Because FRET efficiency is determined by both the orientation and the distance between donor and acceptor proteins, flexible linkers formed from several GGSGSR or GGTGGT repeats were used to determine the optimal distance between the donor and acceptors [46].

3.2. FRET efficiency of the biosensor: acceptor-photobleaching (AP) and fluorescence lifetime imaging microscopy study (FLIM)

The introduction of linkers with adjustable lengths allowed the rapid creation of biosensor variants with varied distances between fluorescent proteins. Thirty-eight biosensor variants were generated, each with a unique distance between the fluorescent proteins (the distance is indicated on the graph as the number of identical hexapeptides in the LN1 and LN2 linkers; the shortest linkers had only one repeat whereas the longest ones contained eight repeats) and screened with AP to determine their FRET efficiency. Biosensors with the highest FRET efficiency were identified with the AP technique and analyzed using FLIM to confirm the AP-based FRET efficiency measurements. Fig. 1B shows the FRET efficiency values calculated from the AP experiments (red and orange bars). Of these, six (orange bars in Fig. 1B) with FRET efficiency of at least 0.16 were then analyzed in detail using FLIM. Table 1 provides the FRET efficiency values calculated from the FLIM data. The biosensor named 7.1 in Table 1, with seven identical segments in the LN2 linker (seven GGTGGTTCTGGTTCTAGA repeats in its DNA sequence) and one segment in the LN1 linker (one GGAGGAACCGGTGGAACT repeat in its DNA sequence), had the highest FRET efficiency. The FRET efficiency determined using AP (Fig. 1C) and FLIM was found to be $Ef_D = 0.20 \pm 0.03$ and $Ef_D = 0.23 \pm 0.04$ (Table 1), respectively. The analysis of the fluorescence emission spectra at donor excitation gathered prior to and after AP also confirmed the occurrence of FRET in the optimized biosensor (Fig. 1C and D). The relative contribution of mTFP1 (donor peak in Fig. 1D) increased following AP whereas the fluorescence of Venus (acceptor peak in Fig. 1D) significantly diminished.

Once the linker lengths were optimized, the influence of the secondary and tertiary structures of the region that contained the MMP-9 cleavage site on cleavage efficiency was explored. Chen et al. [47] sought to develop genetically encoded fluorescent

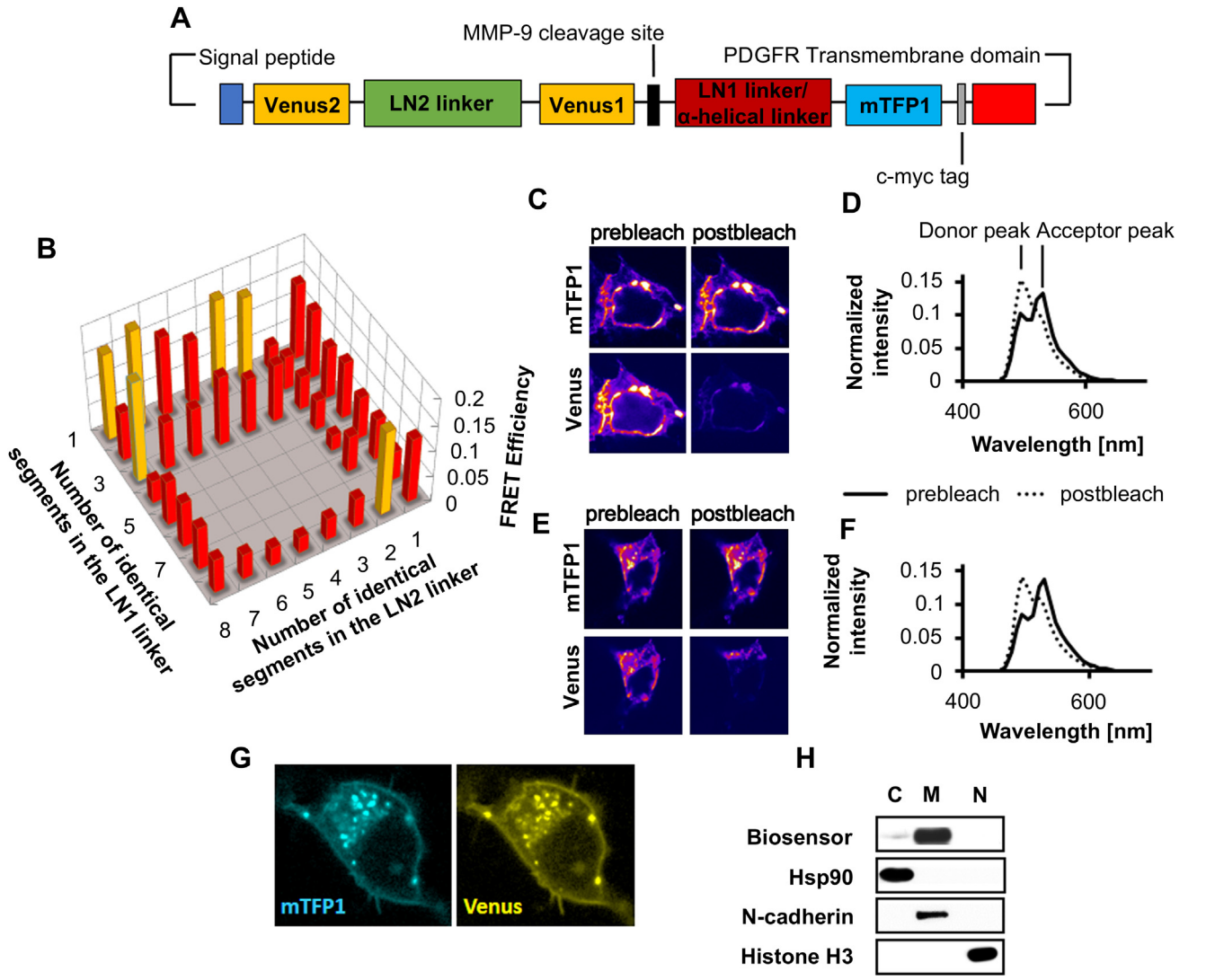

Fig. 1. The construction and optimization of the FRET-based MMP-9 activity biosensor. **A** – Schematic representation of the MMP-9 activity biosensors generated during the entire course of the study. Venus proteins are separated by an LN2 linker (1–8 GGSGSR repeats), and Venus and mTFP1 are separated by an MMP-9 cleavage site (N′-PRSLS-C′) and LN1 linker (1–8 GGTGGT repeats). The c-myc tag simplifies biosensor detection in the Western blot. The signal peptide directs the biosensor toward the secretory pathway, whereas the PDGFR-transmembrane domain anchors the biosensor within cellular membranes. **B** – FRET efficiency values of biosensor variants calculated from Acceptor-Photobleaching observations. Red and orange bars indicate the FRET efficiency of each biosensor variant identified by the number identical segments in each linker. Orange bars indicate biosensor variants analyzed with Fluorescence Lifetime Imaging Microscopy. **C** – Acceptor-Photobleaching of a HEK293 cell that expressed the linker-length optimized biosensor (called 7.1) with a loop-like linker. Following AP, the fluorescence of mTFP1 increased, confirming FRET. **D** – Fluorescence emission spectra of the biosensor imaged in 1C before and after AP. Following AP, the relative contribution of mTFP1 increased (donor peak), whereas the contribution of Venus diminished (acceptor peak), confirming the presence of FRET. **E** – Acceptor-Photobleaching of a HEK293 cell that expressed the biosensor with the α-helical linker. mTFP1 fluorescence increased following AP, confirming the presence of FRET in an unbleached biosensor. **F** – Fluorescence emission spectra of the biosensor imaged in 1E. Following AP, the relative contribution of mTFP1 increased, whereas the contribution of Venus decreased, confirming the presence of FRET in an unbleached biosensor. **G** – Live-cell imaging of a HEK293 cell that expressed the biosensor. The plasma membrane is visible as a narrow band of higher fluorescence that surrounds the cell. **H** – Fractionation results of the HEK293 cell line that expressed the biosensor. Cytoplasmic (C), cellular membranes (M) and nuclear (N) fractions were collected. The biosensor is present only in the cytoplasmic and cellular membranes fraction, with the majority localized in the cellular membranes. Anti-c-myc tag antibody was used to detect the biosensor. Fraction purity was tested using the following fraction markers: hsp90 (chaperon, cytoplasm marker), N-cadherin (transmembrane protein, plasma membrane marker) and histone H3 (DNA binding protein, nucleus marker). (For interpretation of the references to color in this figure legend, the reader is referred to the web version of this article.)

biosensors for the detection of protease activity and suggested that the inclusion of α-helices within the cleavage region increases the accessibility of a cleavage site to proteases. The biosensor with a loop-like LN1 linker was modified by placing the MMP-9 cleavage site between two α-helices. Care was taken to ensure that the α-helical linker had an identical length to the loop-like LN1 in terms of amino acid number. The biosensor with an α-helical linker has higher acquisition-bleaching-corrected apparent FRET efficiency compared with the biosensor with the loop-like linker, which was found to be 0.26 ± 0.02 (result based on AP; Fig. 1E and F). The fluorescence emission spectra of the biosensor with the α-helical

Table 1
FLIM results for the biosensor variants with the highest FRET efficiencies in the AP experiments. FRET efficiency values calculated in FLIM experiments are given. Error values were estimated using the Gaussian noise propagation equation.

FRET efficiency of MMP-9 activity biosensor variants with loop-like linker – FLIM data					
3.1[a]	4.1	7.1	8.1	8.3	2.8
22 ± 4%	22 ± 4%	23 ± 4%	19 ± 4%	20 ± 4%	22 ± 4%

[a] The biosensors (e.g., 3.1, 4.1) are named as follows: the first number denotes the number of identical repeats in the LN2 linker, the second number denotes the number of identical repeats in the LN1 linker.

linker gathered before and after AP (Fig. 1F) also confirmed the presence of FRET. Given the higher FRET efficiency exhibited by the biosensor with the α-helical linker, it was used in further studies.

3.3. Cellular membrane localization

As expected from the PDGF receptor anchor employed, the MMP-9 activity biosensor was localized at the plasma membrane. This was confirmed by direct visualization using confocal microscopy of living HEK293 cells that expressed the biosensor (Fig. 1G) and through cell fractionation followed by Western blot analysis of the collected fractions (Fig. 1H). Three fractions were collected: cytoplasm (C), cellular membranes (M), and nucleus (N). Fraction purity was tested using fraction markers: hsp90 (chaperon, cytoplasm marker), N-cadherin (transmembrane protein, plasma membrane marker) and histone H3 (DNA binding protein, nucleus marker). The biosensor was detected using anti-GFP antibody. Densitometric analysis of the Western blot data revealed that 87 ± 6% of the biosensor was located within cellular membranes and a small percentage was located in the cytoplasm. No biosensor was observed in the nucleus.

3.4. In vitro biosensor cleavage

The MMP-9 activity biosensor was cleaved *in vitro* by a recombinant auto-activating (aa) MMP-9 (Fig. 2A). A gradual decrease in the level of the full-length biosensor was observed over time, with approximately 50% cleaved within 1 h (Fig. 2A, lower panel). Cleavage was blocked by the addition of a broad-spectrum MMP inhibitor, GM6001 (Fig. 2C). Densitometric analysis of the control lane (Fig. 2B) revealed that the biosensor was already partially cleaved (14.2 ± 0.4%; value normalized to the intensity of a full length biosensor band) in transfected but otherwise untreated HEK293 cells. This *in vitro basal* cleavage of the biosensor with the α-helical linker was not attributable to the spontaneous degradation of the protein (incubation with GM6001 blocks cleavage). A slight increase in the amount of a cleaved form of the biosensor was observed over time (Fig. 2B, baseline part of the gel). Basal cleavage was likely caused by endogenous MMP-9 present in the HEK293 extract used as a source of the biosensor. Inactive (in) MMP-9 did not cleave the biosensor (Fig. 2B), demonstrated by the similarity of the time course of MMP-9 cleavage to baseline cleavage.

The cleavage of the biosensor upon MMP-9 treatment was verified in fixed HEK293 cell cultures. Fluorescence emission spectra collected from the plasma membrane of biosensor-expressing HEK293 cells (Fig. 3, inset) incubated with aaMMP-9 for 30 min confirmed that the biosensor was cleaved in the cellular membrane (Fig. 3). The biosensor cleavage could be observed as a change in the emission spectrum of the biosensor within the membrane. Treatment with aaMMP-9 resulted in a shift of the spectrum toward shorter wavelengths, a decrease in the contribution of Venus fluorescence (acceptor peak) to the fluorescence signal, and a corresponding increase in mTFP1 contribution (donor peak).

3.5. Biosensor cleavage in living cells

To verify whether the biosensor is cleaved in living cells, live-cell imaging of HEK293 cells was performed (Fig. 4). MMP-9 induced cleavage of the sensor was observed as a decrease in the Venus-to-mTFP1 fluorescence intensity ratio (intact, high ratio; cleaved, low ratio) in Fig. 4A and B. This method, based on measurements of the emission ratio after single short-wavelength excitation, is optimal in terms of the signal-to-noise ratio, if only relative changes of the

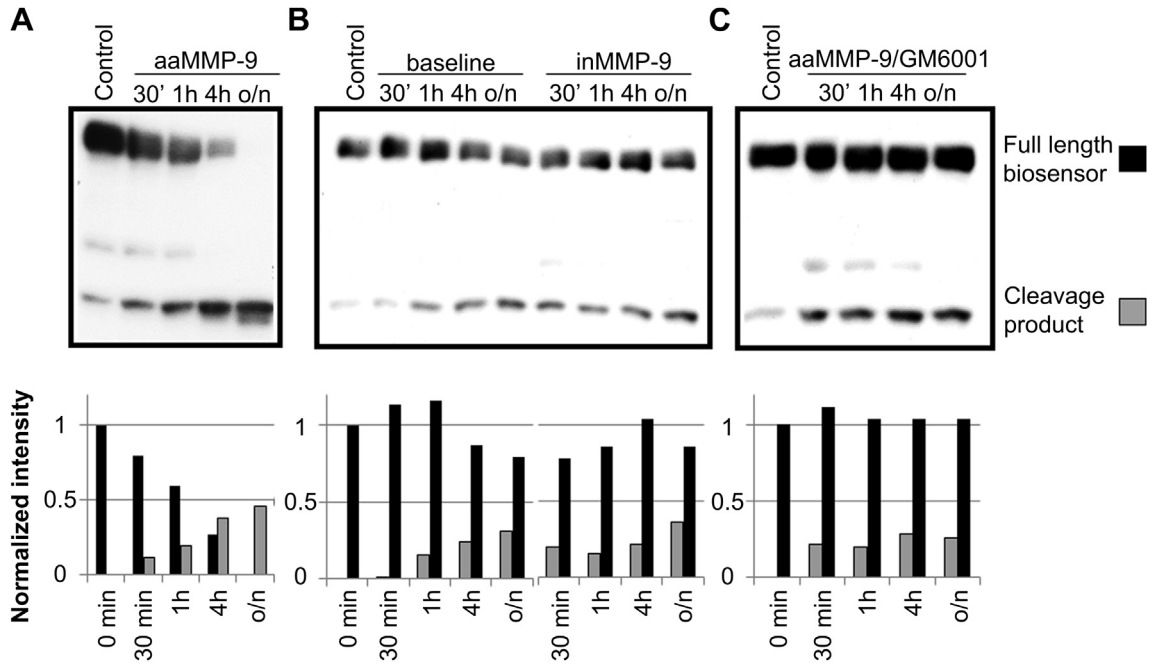

Fig. 2. *In vitro* cleavage of the biosensor with an α-helical linker. **A** – Time course (30 min, 1 h, 2 h, 4 h, and overnight cleavage) of aaMMP-9 cleavage of the biosensor (upper panel) and quantification (lower panel; black bars, normalized intensity of a full-length biosensor band on the corresponding gel lane; gray bar, normalized intensity of a cleaved form of a biosensor). Auto-activating MMP-9 cleaved the biosensor. **B** – Time course of baseline cleavage of the biosensor by any proteases present in the cell extract (left part of the picture) and time course of biosensor incubation with inMMP-9. A slight increase in the amount of cleaved biosensor was observed over time (quantification plots in the lower part of the panel) in both the baseline and inMMP-9 experiments, most likely caused by endogenous MMP-9 present in the cell extract. **C** – Effect of the broad-spectrum MMP inhibitor GM6001 on biosensor cleavage by MMP-9. GM6001 at a concentration of 25 μM blocked the activity of both aaMMP-9 and endogenous MMPs. The biosensor was detected with the anti-GFP antibody. In the quantification plots, intensity was normalized to the full-length biosensor in the control lanes. The intensity of the cleavage product in the control lane was subtracted from the cleavage product intensities in the 30 min, 1 h, 4 h and overnight cleavage lanes prior to normalization.

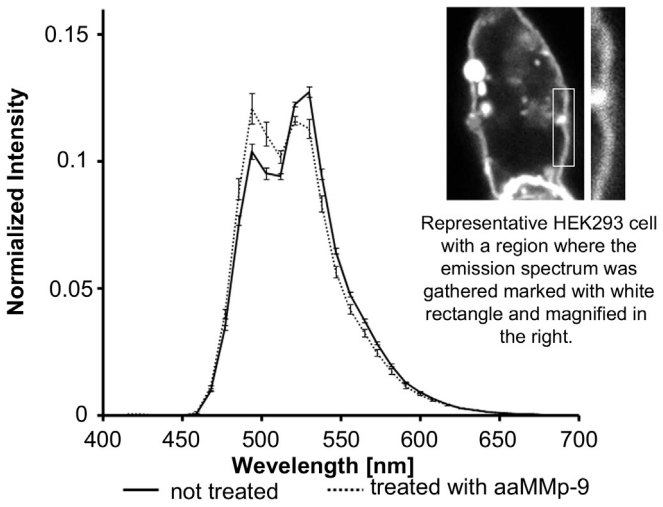

Fig. 3. Treatment of HEK293 cells that expressed the biosensor with an α-helical linker with aaMMP-9 caused a shift of the fluorescence emission spectrum of the biosensor toward shorter wavelengths indicating cleavage of the biosensor. Fluorescence emission spectra were collected from fixed cells. The emission spectrum of a biosensor cleaved by aaMMP-9 had a larger contribution of mTFP1 fluorescence, with a diminished contribution of Venus compared with the emission spectrum of a biosensor that was not cleaved by MMP-9. Inset – Maximum projection of a representative lambda stack of a HEK293 cell that expressed the biosensor. The white rectangle indicates an approximate region of interest (ROI) from which the emission spectrum was acquired. The right part of the inset shows a magnified view of the ROI. For each cell, three ROIs were used to calculate the average emission spectrum. Error bars represent SEM values. $N = 32$.

ratio are of interest [48]. Fluorescence intensity ratio values across the cell surface at different time points of the experiment are indicated by red-shifted (high ratio values) and blue-shifted (low ratio values) colors (Fig. 4A) and in normalized Venus-to-mTFP1 fluorescence intensity ratio traces (Fig. 4B). The fluorescence intensity ratio began decreasing several minutes after the addition of aaMMP-9. Mock treatment with pure medium (Fig. 4B) or treatment with inMMP-9 (Fig. 4B) did not lead to a change in the Venus-to-mTFP1 fluorescence intensity ratio, which remained relatively constant throughout the experiment (Fig. 4B).

The experiment was repeated with rat hippocampal neurons treated with aaMMP-9 or stimulated with the cLTP mixture (see Materials and Methods) to evoke endogenous MMP-9 release. The addition of aaMMP-9 to the cell culture (Fig. 5A; the colors correspond to the value of the fluorescence intensity ratio, with a higher ratio indicated by red-shifted colors and a low ratio indicated by blue-shifted colors) closely mirrored the results obtained with the HEK293 cell line. The decrease in the Venus-to-mTFP1 intensity ratio following aaMMP-9 treatment became statistically significant compared with mock treatment 9 min after the addition of MMP-9 onward ($p < 0.05$ at 9 min after stimulation, $p < 0.01$ at 14 min after stimulation). The cLTP protocol that selectively upregulates MMP-9 gelatinase activity [26] also led to the cleavage of the biosensor (Fig. 5B). cLTP-induced cleavage of the biosensor achieved statistical significance compared with mock treatment 10 min after the addition of the cLTP mixture ($p < 0.05$ at 10 min after stimulation, $p < 0.01$ at 21 min after stimulation), whereas the response of the biosensor to aaMMP-9 and cLTP remained similar until 25 min after aaMMP-9 and cLTP treatment, when they began to differ

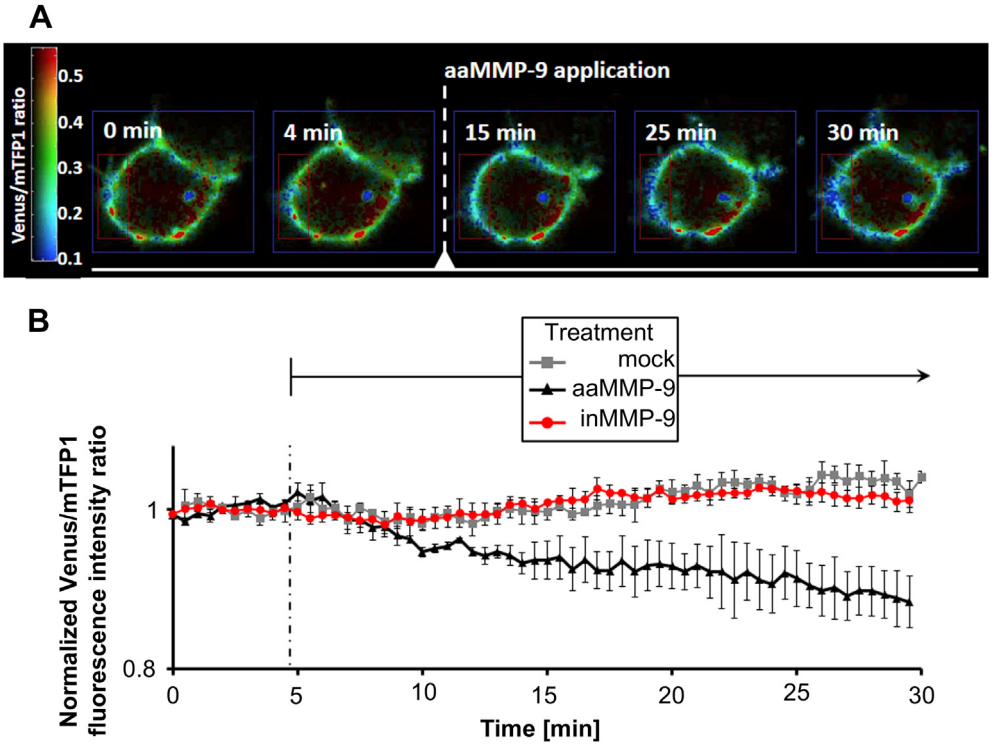

Fig. 4. Live imaging of a HEK293 cells that expressed the biosensor with an α-helical linker. The time course of acceptor-to-donor fluorescence intensity ratios upon cell stimulation is shown. **A** – Fluorescence intensity ratio values across the cell surface at different time-points of the experiment are indicated by red-shifted (high ratio values) and blue-shifted (low ratio values) colors. A map that correlates the fluorescence intensity ratio values (OY axis) with the color assigned to that value and fluorescence intensity in that pixel (OX axis) is to the left. Darker colors indicate that the fluorescence intensity was closer to background levels. Warmer colors indicate higher fluorescence intensity ratios. aaMMP-9 was added to the culture at the 5 min time-point. Notice the gradual shift of the colors toward colder hues (lower ratio values), indicating cleavage of the biosensor by aaMMP-9. **B** – Fluorescence intensity ratios of cells mock-treated (gray line), treated with inMMP-9 (red line), or treated with aaMMP-9 (black line) were normalized to an average fluorescence intensity ratio calculated for time-points before the start of the treatment. Each line represents an averaged intensity ratio of three cells. Notice the gradual decrease in the fluorescence intensity ratios of cells treated with aaMMP-9. No such decrease was observed in cells that were either mock treated or treated with inMMP-9. Error bars represent SEM values. $N = 60$. (For interpretation of the references to color in this figure legend, the reader is referred to the web version of this article.)

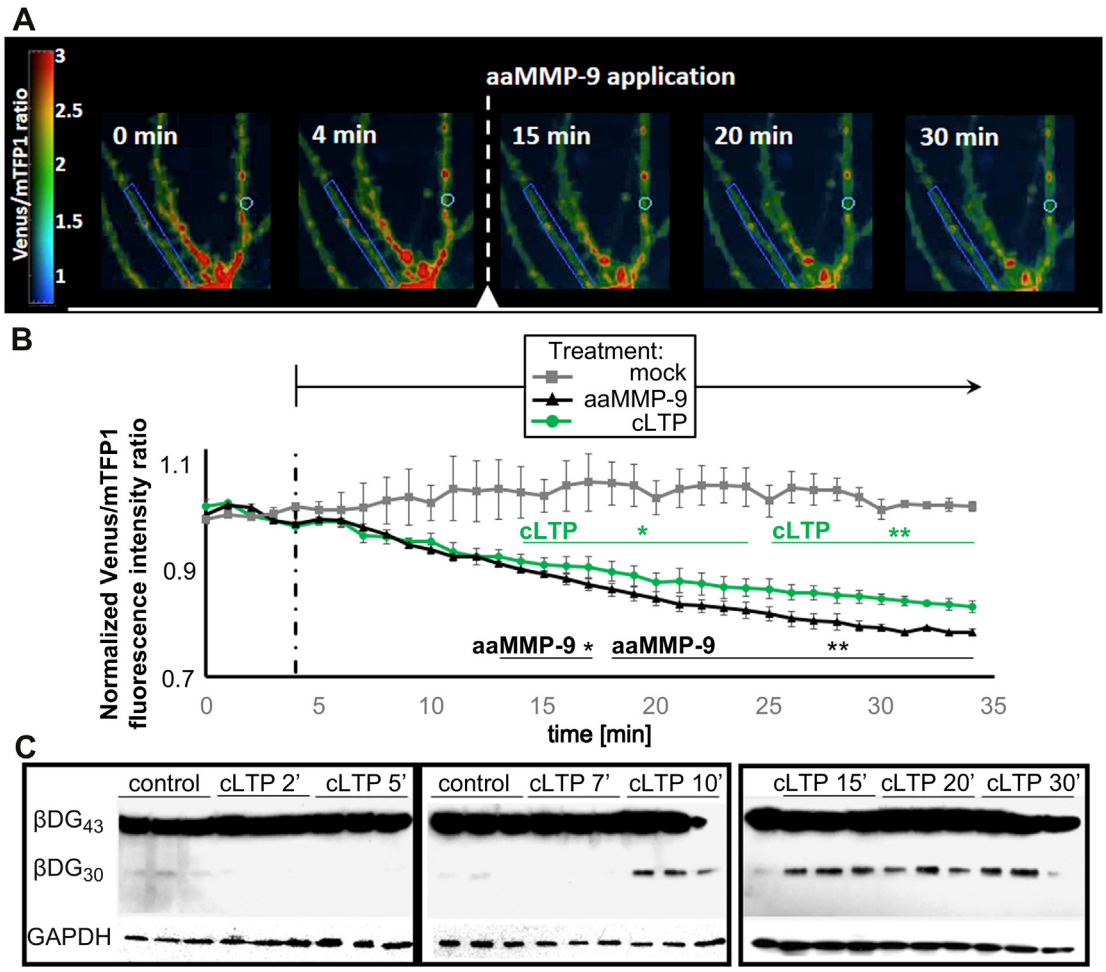

Fig. 5. Live-cell imaging of hippocampal primary neurons that expressed the biosensor with an α-helical linker. **A** – Magnified view of a neuron treated with aaMMP-9. Colors indicate fluorescence intensity ratios (for precise descriptions of the colors, see the color map to the left). Notice the gradual shift of colors toward colder hues, indicating biosensor cleavage. **B** – Fluorescence intensity ratios of cells mock-treated (gray line), incubated with aaMMP-9 (black line), or undergoing cLTP (green line). The data were normalized to the averaged ratio prior to stimulation. aaMMP-9 and endogenous MMP-9 (release caused by cLTP) caused a decrease in the Venus-to-mTFP1 intensity ratio, indicating biosensor cleavage. Each line represents an averaged intensity ratio of three cells. Error bars represent SEM values. $N = 35$. *t*-tests were performed to assess the statistical significance of aaMMP-9 and cLTP treatments compared with the mock treatment). aaMMP-9: $0.01 < p < 0.05$ for 13–17 min, $p < 0.01$ for 18–34 min; cLTP: $0.01 < p < 0.05$ for 14–24 min, $p < 0.01$ for 25–34 min. **C** – Kinetics of βDG cleavage upon cLTP stimulation of a primary culture. MMP-9 cleavage of the 43 kDa protein led to the release of a 30 kDa partial cleavage product. GAPDH was given as a loading control. Cleavage products first appeared 10 min after cLTP stimulation, supporting the results obtained in the live-cell imaging of hippocampal neurons stimulated with the cLTP mixture. (For interpretation of the references to color in this figure legend, the reader is referred to the web version of this article.)

significantly ($p < 0.02$ at 25 min after treatment, $p < 0.01$ at 27 min after treatment).

To support the MMP-9 activity kinetics data upon cLTP obtained with the use of the biosensor, MMP-9 kinetics were further measured using the β-dystroglycan (βDG) cleavage assay. βDG was identified previously [41] as an *in vivo* substrate of MMP-9 that is cleaved in response to enhanced neuronal activity. Szepesi et al. [26] observed βDG cleavage following the upregulation of endogenous MMP-9 activity caused by chemically induced LTP, providing an easy way to verify the MMP-9 kinetics obtained with the biosensor. βDG cleavage in primary cultures after cLTP was first observable approximately 10 min after the beginning of stimulation (Fig. 5C), which is consistent the biosensor cleavage kinetics following cLTP in living neurons.

4. Discussion

In the present study, a biosensor that measures the enzymatic activity of MMP-9 was described. The biosensor utilizes a cyan fluorescent protein mTFP1, that possesses superior spectral properties compared with CFP [45], namely increased brightness and improved spectral overlap with Venus. mTFP1 serves as an energy donor, and two Venus proteins serve as energy acceptors. The distance between fluorescent proteins was optimized to maximize the effective FRET efficiency. Through AP- and FLIM-based FRET analysis of several biosensor variants that differed in the distance between fluorescent proteins, we determined that an LN2 linker that contains seven GGSGSR repeats between Venus1 and Venus2 and an LN1 linker that contains the MMP-9 cleavage site and one hexapeptide GGTGGT repeat are optimal. This biosensor variant, internally referred to as 7.1, was found to have $E_{fD} = 0.20 \pm 0.03$ (AP data) and $E_{fD} = 0.23 \pm 0.04$ (FLIM data). The effect of a secondary structure of the linker on MMP-9 cleavage efficiency was also investigated. The MMP-9 protease cleaved the biosensor more efficiently when the cleavage site was located within the α-helix. Unexpectedly, the biosensor with the α-helical linker displayed a higher FRET efficiency ($E_{fD} = 0.26 \pm 0.02$) than the biosensor with a loop-like linker, which likely results from different secondary structures assumed by loop-like and α-helical linkers, with the latter being more compact and thus bringing the

donor and acceptors closer to each other. The MMP-9 cleavage site cloned into the biosensor was based on a consensus sequence of a large group of MMP-9-cleavable peptides [37]. The specificity of the cleavage site was shown previously [27,38], using human recombinant MMP-2, MMP-3, and MMP-7.

We demonstrated that the proteolytic activity of MMP-9 leads to the release of dual Venus proteins from the cell membrane and a decrease in the Venus-to-mTFP1 fluorescence intensity ratio. The biosensor was present predominantly in cellular membranes ($87 \pm 6\%$) and cleaved by MMP-9 in the *in vitro* assay. We showed that the cleavage was not attributable to spontaneous degradation of the biosensor, and it can be blocked by the addition of a broad-spectrum MMP inhibitor. The baseline cleavage of the biosensor was observable in untreated lysate. Cell lysis was performed without protease inhibitors of any kind, and the observed cleavage may be caused by endogenous MMP-9 present in the HEK293 cell lysate. The data suggest that this baseline cleavage was blocked by a broad spectrum MMP inhibitor GM6001.

To image MMP-9 activity, fluorescence emission spectra were collected from cell membranes of HEK293 cells that expressed the biosensor. The cells were treated with the aaMMP-9, fixed, and the fluorescence emission spectra were collected. These spectra differed from those recorded from untreated cells. The contribution of mTFP1 to the fluorescence signal increased, implying cleavage of the biosensor. The effect of MMP-9 on the structure of the biosensor was also followed by live-cell imaging microscopy. The treatment of HEK293 cells with aaMMP-9 led to a steady decrease in the Venus-to-mTFP1 fluorescence intensity ratio, whereas mock treatment with pure medium and treatment with inMMP-9 did not lead to any significant changes in the ratio. We previously reported that the cLTP protocol [26] selectively upregulated MMP-9 gelatinase activity at 10 min post-stimulation. Additionally, Niedringhaus et al. [49] observed enhanced neuronal activity of cultured hippocampal neurons following cLTP. Live-cell imaging performed with rat hippocampal neurons transfected with the biosensor following cLTP revealed the detailed kinetics of MMP-9 activity that closely mimicked the kinetics of βDG cleavage as observed using Western blot. The ratiometric method based on calculating the acceptor-to-donor emission ratio after a single-wavelength excitation, revealed statistically significant upregulation of endogenous MMP-9 activity 9 min after cLTP stimulation.

Understanding various functions performed by MMP-9 under physiological conditions (e.g., extracellular matrix remodeling, angiogenesis and synaptic plasticity) and pathological conditions (e.g., malignant progression of tumors and epilepsy) requires tools that enable the assessment of its proteolytic activity. Recent years have witnessed the development of numerous functional imaging techniques that provide the means to localize and measure MMP-9 activity in living cells. All of these methods depend on an exogenously applied fluorescent probe that can be cleaved by MMP-9. A genetically encoded, membrane-anchored, FRET-based MMP-9 activity biosensor might be better suited to elucidate the role of the proteolytic activity of MMP-9 in physiological and pathological processes.

The genetically encoded FRET-based biosensor of MMP-9 activity began to be recognized [50] as a tool that is essential for understanding the molecular mechanics of long-term memory storage. The biosensor described herein responds to this need. Recent studies have shown that MMP-9 plays a critical role in the physiology of the brain. Although probes such as DQ-gelatin have been useful for studying that aspect of the role of MMP-9, they do not offer the required spatiotemporal resolution needed to answer numerous questions that have since arisen.

5. Conclusions

We have developed a nontoxic genetically encoded MMP-9 activity biosensor that is anchored in the cellular membrane and thus has an important advantage over currently employed probes. Our approach to detect MMP-9 activity overcomes the current generation of MMP-9 activity probes that lack the resolution needed to reveal the precise function of MMP-9 within the organism. The biosensor enables the study of the proteolytic activity of MMP-9 with high temporal and subcellular resolution at the precise region of MMP-9 action on the cell. The biosensor functionality was demonstrated both *in vitro* and living cells.

Acknowledgments

Research was supported by ERA-NET NEURON MODDIFSYN and the National Science Centre (Dec-2011/01/D/NZ3/00163). This work was also partially supported by TEAM/2011-8/3 programme of Foundation for Polish Science, co-financed from European Union, Regional Development Fund (I R-W, L K).

References

[1] Miranda JG, Weaver AL, Qin Y, Park JG, Stoddard CI, Lin MZ, et al. New alternately colored FRET sensors for simultaneous monitoring of Zn^{2+} in multiple cellular locations. PLoS One 2012;7:e49371.
[2] Burdette SC, Walkup GK, Spingler B, Tsien RY, Lippard SJ. Fluorescent sensors for Zn2+ based on a fluorescein platform: synthesis, properties and intracellular distribution. J Am Chem Soc 2001;123:7831–41.
[3] Esposito A, Gralle M, Dani MAC, Lange D, Wouters FS. pHlameleons: a family of FRET-based protein sensors for quantitative pH imaging. Biochemistry 2008;47:13115–26.
[4] Gruenwald K, Holland JT, Stromberg V, Ahmad A, Watcharakichkorn D, Okumoto S. Visualization of glutamine transporter activities in living cells using genetically encoded glutamine sensors. PLoS One 2012;7:e38591.
[5] Kaláb P, Soderholm J. The design of Förster (fluorescence) resonance energy transfer (FRET)-based molecular sensors for Ran GTPase. Methods 2010;51:220–32.
[6] Violin JD, Zhang J, Tsien RY, Newton AC. A genetically encoded fluorescent reporter reveals oscillatory phosphorylation by protein kinase C. J Cell Biol 2003;161:899–909.
[7] Meng F, Sachs F. Visualizing dynamic cytoplasmic forces with a compliance-matched FRET sensor. J Cell Sci 2011;124:261–9.
[8] Klein T, Bischoff R. Physiology and pathophysiology of matrix metalloproteases. Amino Acids 2011;41:271–90.
[9] Deryugina EI, Quigley JP. Matrix metalloproteinases and tumor metastasis. Cancer Metastasis Rev 2006;25:9–34.
[10] Kessenbrock K, Plaks V, Werb Z. Matrix metalloproteinases: regulators of the tumor microenvironment. Cell 2010;141:52–67.
[11] Hanemaaijer R, Verheijen JH, Maguire TM, Visser H, Toet K, McDermott E, et al. Increased gelatinase-A and gelatinase-B activities in malignant vs. benign breast tumors. Int J Cancer 2000;86:204–7.
[12] Schmalfeldt B, Prechtel D, Härting K, Späthe K, Rutke S, Konik E, et al. Increased expression of matrix metalloproteinases (MMP)-2, MMP-9, and the urokinase-type plasminogen activator is associated with progression from benign to advanced ovarian cancer. Clin Cancer Res 2001;7:2396–404.
[13] Schönbeck U, Mach F, Libby P. Generation of biologically active IL-1β by matrix metalloproteinases: a novel caspase-1-independent pathway of IL-1β processing. J Immunol 1998;161:3340–6.
[14] Yu Q, Stamenkovic I. Cell surface-localized matrix metalloproteinase-9 proteolytically activates TGF-β and promotes tumor invasion and angiogenesis. Genes Dev 2000;14:163–76.
[15] Klein G, Vellenga E, Fraaije MW, Kamps WA, de Bont ES. The possible role of matrix metalloproteinase (MMP)-2 and MMP-9 in cancer, e.g. acute leukemia. Crit Rev Oncol Hematol 2004;50:87–100.
[16] Bozdagi O, Nagy V, Kwei KT, Huntley GW. In vivo roles for matrix metalloproteinase-9 in mature hippocampal synaptic physiology and plasticity. J Neurophysiol 2007;98:334–44.
[17] Nagy V, Bozdagi O, Matynia A, Balcerzyk M, Okulski P, Dzwonek J, et al. Matrix metalloproteinase-9 is required for hippocampal late-phase long-term potentiation and memory. J Neurosci 2006;26:1923–34.
[18] Okulski P, Jay TM, Jaworski J, Duniec K, Dzwonek J, Konopacki FA, et al. TIMP-1 abolishes MMP-9-dependent long-lasting long-term potentiation in the prefrontal cortex. Biol Psychiatry 2007;62:359–62.
[19] Huntley GW. Synaptic circuit remodelling by matrix metalloproteinases in health and disease. Nat Rev Neurosci 2012;13:743–57.

[20] Bilousova TV, Dansie L, Ngo M, Aye J, Charles JR, Ethell DW, et al. Minocycline promotes dendritic spine maturation and improves behavioural performance in the fragile X mouse model. J Med Genet 2009;46:94–102.
[21] Michaluk P, Wawrzyniak M, Alot P, Szczot M, Wyrembek P, Mercik K, et al. Influence of matrix metalloproteinase MMP-9 on dendritic spine morphology. J Cell Sci 2011;124:3369–80.
[22] Wang XB, Bozdagi O, Nikitczuk JS, Zhai ZW, Zhou Q, Huntley GW. Extracellular proteolysis by matrix metalloproteinase-9 drives dendritic spine enlargement and long-term potentiation coordinately. Proc Natl Acad Sci U S A 2008;105:19520–5.
[23] Wlodarczyk J, Mukhina I, Kaczmarek L, Dityatev A. Extracellular matrix molecules, their receptors, and secreted proteases in synaptic plasticity. Dev Neurobiol 2011;71:1040–53.
[24] Szklarczyk A, Lapinska J, Rylski M, McKay RDG, Kaczmarek L. Matrix metalloproteinase-9 undergoes expression and activation during dendritic remodeling in adult hippocampus. J Neurosci 2002;22:920–30.
[25] Wilczynski GM, Konopacki FA, Wilczek E, Lasiecka Z, Gorlewicz A, Michaluk P, et al. Important role of matrix metalloproteinase 9 in epileptogenesis. J Cell Biol 2008;180:1021–35.
[26] Szepesi Z, Bijata M, Ruszczycki B, Kaczmarek L, Wlodarczyk J. Matrix metalloproteinases regulate the formation of dendritic spine head protrusions during chemically induced long-term potentiation. PLoS One 2013;8:e63314.
[27] Fudala R, Ranjan AP, Mukerjee A, Vishwanatha JK, Gryczynski Z, Borejdo J, et al. Fluorescence detection of MMP-9. I. MMP-9 selectively cleaves Lys-Gly-Pro-Arg-Ser-Leu-Ser-Gly-Lys peptide. Curr Pharm Biotechnol 2011;12:834–8.
[28] Akers WJ, Xu B, Lee H, Sudlow GP, Fields GB, Achilefu S, et al. Detection of MMP-2 and MMP-9 activity in vivo with a triple-helical peptide optical probe. Bioconjug Chem 2012;23:656–63.
[29] Roopali Roy DZ, Pories Susan, Moss Marcia L, Moses Marsha A. Potential of fluorescent metalloproteinase substrates for cancer detection. Clin Biochem 2011;44:1434–9.
[30] Hawkins KE, Demars KM, Yang C, Rosenberg GA, Candelario-Jalil E. Fluorometric immunocapture assay for the specific measurement of matrix metalloproteinase-9 activity in biological samples: application to brain and plasma from rats with ischemic stroke. Mol Brain 2013;6:14.
[31] Leight JL, Alge DL, Maier AJ, Anseth KS. Direct measurement of matrix metalloproteinase activity in 3D cellular microenvironments using a fluorogenic peptide substrate. Biomaterials 2013;34:7344–52.
[32] Wang W, Shao R, Wu Q, Ke S, McMurray J, Lang Jr F, et al. Targeting gelatinases with a near-infrared fluorescent cyclic His-Try-Gly-Phe peptide. Mol Imaging Biol 2009;11:424–33.
[33] Scherer R, McIntyre JO, Matrisian L. Imaging matrix metalloproteinases in cancer. Cancer Metastasis Rev 2008;27:679–90.
[34] Lee C-M, Jang D, Cheong S-J, Jeong M-H, Kim E-M, Kim DW, et al. Optical imaging of MMP expression and cancer progression in an inflammation-induced colon cancer model. Int J Cancer 2012;131:1846–53.
[35] Kaijzel EL, van Heijningen PM, Wielopolski PA, Vermeij M, Koning GA, van Cappellen WA, et al. Multimodality imaging reveals a gradual increase in matrix metalloproteinase activity at aneurysmal lesions in live fibulin-4 mice. Circ Cardiovasc Imaging 2010;3:567–77.
[36] Wallis de Vries BM, Hillebrands J-L, van Dam GM, Tio RA, de Jong JS, Slart RHJA, et al. Multispectral near-infrared fluorescence molecular imaging of matrix metalloproteinases in a human carotid plaque using a matrix-degrading metalloproteinase–sensitive activatable fluorescent probe. Circulation 2009;119:e534–6.
[37] Kridel SJ, Chen E, Kotra LP, Howard EW, Mobashery S, Smith JW. Substrate hydrolysis by matrix metalloproteinase-9. J Biol Chem 2001;276:20572–8.
[38] Fudala R, Mukerjee A, Ranjan AP, Vishwanatha JK, Kurdowska AK, Gryczynski Z, et al. Fluorescence detection of MMP-9.II. Ratiometric FRET-based sensing with dually labeled specific peptide. Curr Pharm Biotechnol 2012.
[39] Nagai T, Ibata K, Park ES, Kubota M, Mikoshiba K, Miyawaki A. A variant of yellow fluorescent protein with fast and efficient maturation for cell-biological applications. Nat Biotechnol 2002;20:87–90.
[40] Li MZ, Elledge SJ. Harnessing homologous recombination in vitro to generate recombinant DNA via SLIC. Nat Methods 2007;4:251–6.
[41] Michaluk P, Kolodziej L, Mioduszewska B, Wilczynski GM, Dzwonek J, Jaworski J, et al. β-Dystroglycan as a target for MMP-9, in response to enhanced neuronal activity. J Biol Chem 2007;282:16036–41.
[42] Michaluk P, Mikasova L, Groc L, Frischknecht R, Choquet D, Kaczmarek L. Matrix metalloproteinase-9 controls NMDA receptor surface diffusion through integrin β1 signaling. J Neurosci 2009;29:6007–12.
[43] Otmakhov N, Khibnik L, Otmakhova N, Carpenter S, Riahi S, Asrican B, et al. Forskolin-induced LTP in the CA1 hippocampal region is NMDA receptor dependent. J Neurophysiol 2004;91:1955–62.
[44] Zeug A, Woehler A, Neher E, Ponimaskin Evgeni G. Quantitative intensity-based FRET approaches a comparative snapshot. Biophys J 2012;103:1821–7.
[45] Day RN, Booker CF, Periasamy A. Characterization of an improved donor fluorescent protein for Förster resonance energy transfer microscopy. J Biomed Opt 2008;13:031203.
[46] Evers TH, van Dongen EMWM, Faesen AC, Meijer EW, Merkx M. Quantitative understanding of the energy transfer between fluorescent proteins connected via flexible peptide linkers. Biochemistry 2006;45:13183–92.
[47] Chen N, Zou J, Wang S, Ye Y, Huang Y, Gadda G, et al. Designing protease sensors for real-time imaging of trypsin activation in pancreatic cancer cells. Biochemistry 2009;48:3519–26.
[48] Woehler A, Wlodarczyk J, Neher E. Signal/noise analysis of FRET-based sensors. Biophys J 2010;99:2344–54.
[49] Niedringhaus M, Chen X, Dzakpasu R, Conant K. MMPs and soluble ICAM-5 increase neuronal excitability within in vitro networks of hippocampal neurons. PLoS One 2012;7:e42631.
[50] Tsien RY. Very long-term memories may be stored in the pattern of holes in the perineuronal net. Proc Natl Acad Sci U S A 2013;110:12456–61.